8.2 OBJECT KINETIC MONTE CARLO SIMULATIONS OF RADIATION DAMAGE IN TUNGSTEN—

G. Nandipati, W. Setyawan, H. L. Heinisch, K. J. Roche, R. J. Kurtz (Pacific Northwest National Laboratory) and B. D. Wirth (University of Tennessee)

OBJECTIVE

The objective of this work is to study the radiation damage created by primary knock-on atoms (PKAs) of various energies, at various temperatures in bulk tungsten using the object kinetic Monte Carlo (OKMC) method.

SUMMARY

We used our recently developed lattice-based object kinetic Monte Carlo code; *KSOME* [1] to carryout simulations of radiation damage in bulk tungsten at temperatures of 300, and 2050 K for various dose rates. Displacement cascades generated from molecular dynamics (MD) simulations for PKA energies at 60, 75 and 100 keV provided residual point defect distributions. It was found that the number density of vacancies in the simulation box does not change with dose rate while the number density of vacancy clusters slightly decreases with dose rate indicating that bigger clusters are formed at larger dose rates. At 300 K, although the average vacancy cluster size increases slightly, the vast majority of vacancies exist as mono-vacancies. At 2050 K no accumulation of defects was observed during irradiation over a wide range of dose rates for all PKA energies studied in this work.

PROGRESS AND STATUS

Introduction

Tungsten is considered as the primary solid material choice for divertor components in future fusion reactors due to its high melting point, low sputtering coefficient, high thermal conductivity, low transmutation probability, low tritium retention and good mechanical strength. Bulk tungsten will be exposed to energetic neutrons escaping the plasma. The deuterium-tritium fusion reaction produces neutrons with a characteristic kinetic energy of 14.1 MeV. Collisions of 14.1 MeV neutrons with tungsten atoms produce tungsten primary-knock-on atoms with various recoil energies. PKA atoms then lose the acquired energy to a large extent by displacing other atoms, in a sequence known as a displacement cascade. This process creates defect clusters such as vacancy and self-interstitial atom (SIA) clusters. Creation of point defects and clusters of these defects, subsequent migration, additional clustering and dissolution of clusters results in dramatic microstructural changes during neutron irradiation.

Simulation Details

Simulations were performed on a non-cubic block of tungsten atoms with dimensions 95.1 x 110.95 x 126.8 nm^3, with each axis parallel to a <100> direction of the crystal. Each defect is allowed to hop to one of eight body-centered cubic nearest neighbor lattice sites at *a*/2 (111), where *a* is the lattice constant. Finite periodic boundary conditions were adopted in all three directions i.e. periodic boundary conditions are applied but whenever a mobile object has moved a distance larger than the average grain size, it is removed from the simulation and it is no longer tracked. This approach is physically meaningful because SIA clusters diffuse very fast and reach the grain boundaries very quickly. In the present simulation we used an average grain size of 1 m was used. In these simulations no other traps were considered.

The values of the binding energies of defects used in the present annealing simulations were taken from the *ab initio* calculations of Becquart *et al*. [3] while the migration barriers were taken from MD simulations [4] using an EAM potential for W [5]. In the present simulations SIA clusters larger than size five were constrained to diffuse in 1D along one of four <111> directions. SIA clusters up to size five were allowed to change their direction of 1D motion via rotation and thereby performing mixed 1D/3D motion. The activation barrier for changing direction from one <111> direction to another is 0.38 eV [6]. Since the MD simulations of cascade damage do not provide information on the orientation of SIA diffusion, the direction of 1D motion was assigned randomly to the SIAs at the start of a simulation. Also there is no

information available on the infrequently occurring immobile SIA clusters in these cascades therefore we assumed that all interstitial clusters are glissile (mobile). Their migration/diffusion rates decrease with increasing cluster size (n) according to $\square_o n^{\square 1}$ ($\square_o$ = 6 x 10^{12} s^{-1}) while the migration barrier is independent of cluster size.

For a single vacancy, the activation barrier for diffusion is taken as 1.30 eV [4], and vacancy clusters larger than five are assumed to be immobile. But vacancy clusters of all sizes are allowed to emit mono-vacancies. All mobile vacancy clusters migrate in 3D, and their diffusion rates decrease with cluster size (n) according to $\square_o(q^{-1})^{n-1}$ ($\square_o$ = 6 x 10^{12} s^{-1}, q = 1000) [3]. The vacancy (SIA) dissociation rate is given by $\square_d = \square_d \exp((E_m + E_d)/k_B T)$, where E_d is the binding energy of a vacancy (SIA) to a vacancy (SIA) cluster, and E_m is the migration energy of a single vacancy (SIA). We have assumed that defect clusters of all sizes and types are spherical objects and their capture radii were obtained from Reference [3].

Cascades are randomly selected the database of cascades and inserted into the simulation box at random positions based on the cascade production rate, which depends on the dose rate. In addition, to introduce more variability the coordinates of defects in a cascade are rotated by same amount in random directions around the point of insertion. The production rate of cascades, which is number of cascades produced in the simulation cell per second, and the accumulated dpa (displacements per atom) are calculated based on the NRT displacements per cascade ($\square_{NRT}$) [7], the total number of atoms in the simulation cell of size (N_{atoms}) and the dose rate (dpa/s)

$$\upsilon_{NRT} = 0.8\,\frac{E_{MD}}{2E_D} \qquad (1)$$

Where E_{MD} is the damage energy, i.e the fraction of kinetic energy of the PKA that is not absorbed by electronic excitation, equivalent to the cascade energy in the corresponding MD simulation, and E_D is the displacement threshold energy, which is 128 eV for tungsten [5]. Using the above expression one can calculate dpa per cascade (dpc) as

$$dpc = \frac{\upsilon_{NRT}}{N_{atoms}} \qquad (2)$$

Table 1 shows the NRT displacements per cascade and the dpa per cascade in tungsten at various PKA energies, which is calculated based on the number of atoms in the simulation cell. Total number of atoms in the simulation cell used in the present set of simulations is 84 x 10^6 atoms.

Table 1. NRT displacements per cascade and dpa per cascade in tungsten at various PKA energies

PKA energy (KeV)	**10**	**20**	**30**	**40**	**50**	**60**	**75**	**100**
$\square_{NRT}$	31.25	62.50	93.75	125.0	156.25	187.50	234.38	312.50
dpc (x 10^{-6})	0.372	0.744	1.12	1.49	1.86	2.23	2.79	3.72

Results

A database of 15,15 and 20 cascades at PKA energies of 60, 75 and100 keV respectively, created using MD simulations, was used to carry out these irradiation simulations. The simulations at 300 and 2050 K at dose rates of 10^{-5}, 10^{-6}, 10^{-7} and 10^{-8} dpa s^{-1} and using equations (1) and (2) cascade production rates with 100 keV cascades are 2.7, 0.27, 0.027, 0.0027 cascades per second respectively. To understand the

annealing of single cascades in tungsten we have also collected runtime information like number densities of defects, reaction events (recombination, coalescence, emission, transformation), average cluster sizes and their size distributions, and number densities of defects escaping the box for all the types (in this only SIAs and vacancies) as a function of time. Since this is ongoing work (simulations are still in progress) and simulations at various dose rates are at different levels of defect accumulation, we chose to show the latest information available for a particular dose rate and PKA energy. As mentioned in the introduction, interstitial clusters diffuse very fast and are absorbed by grain boundaries very quickly, leaving only vacancy clusters in the simulation box. Therefore we will only show the vacancy cluster distribution is displayed here.

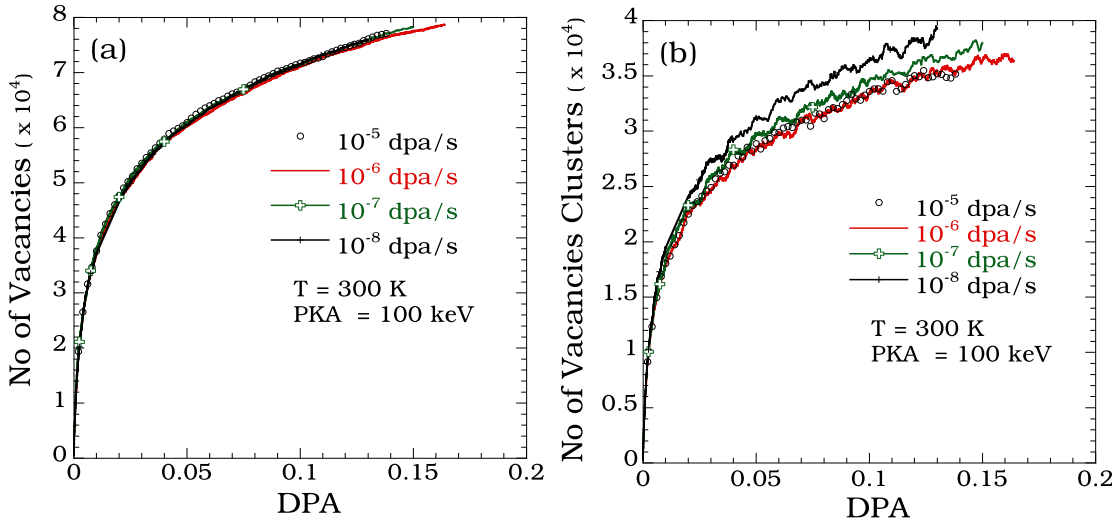

Figure 1. Comparison of damage accumulation at different dose rates using 100 keV cascades at 300 K. (a) Number density of vacancies (b) Number density of vacancy clusters.

Figure 1 shows the plot of the total number of vacancies and vacancy clusters as function of dose at a temperature of 300 K for 100 keV cascades at different dose rates. One can see that there is no noticeable difference in the number density of vacancies but the number density of vacancy clusters decreases with dose rate. Although not shown, the behavior of the number density of vacancies and vacancy clusters at various dose rates is similar for 60 and 75 keV cascades at 300 K.

Figure 2 shows snap shots of the vacancy distributions in the simulation box at various dose rates at 300 K for 100 keV cascades. The radius of each sphere in a snap shot is scaled by the vacancy cluster size as (cluster size)$^{1/3}$. To aid the visualization of the snap shots this radius for each sphere is further increased by 5 times. The coloring scheme for each sphere is based on this new increased radius. It can be seen from Figure 2 that the scale goes from 5 to 26.3882, which corresponds to vacancy cluster sizes from ranging from 1 to 147 vacancies. From Figure 2 it can be seen that at 300 K for 100 keV cascades, most of the vacancies exist as mono-vacancies and are randomly distributed in the simulation cell. Since mono-vacancies are immobile at 300 K most of the large clusters seen in the snap shots are created during cascade production. Again the behavior is very similar for 60 and 75 keV cascades at 300 K (not shown).

At 2050 K for all PKA energies shown in this article, it was found that there was no defect accumulation. At 2050 K, both mono-vacancy diffusion and dissociation of vacancy clusters is active. Therefore all vacancy clusters eventually dissociate into mono-vacancies and diffuse out to the grain boundary before the next cascade is produced. This process is further enhanced by the minimal vacancy clustering in the cascades produced at 2050 K, resulting in no defect accumulation over a wide range of dose rates ranging from 10^{-2} to 10^{-8} dpa s^{-1}. It is likely that this would be true even for other PKA energies not shown in this report.

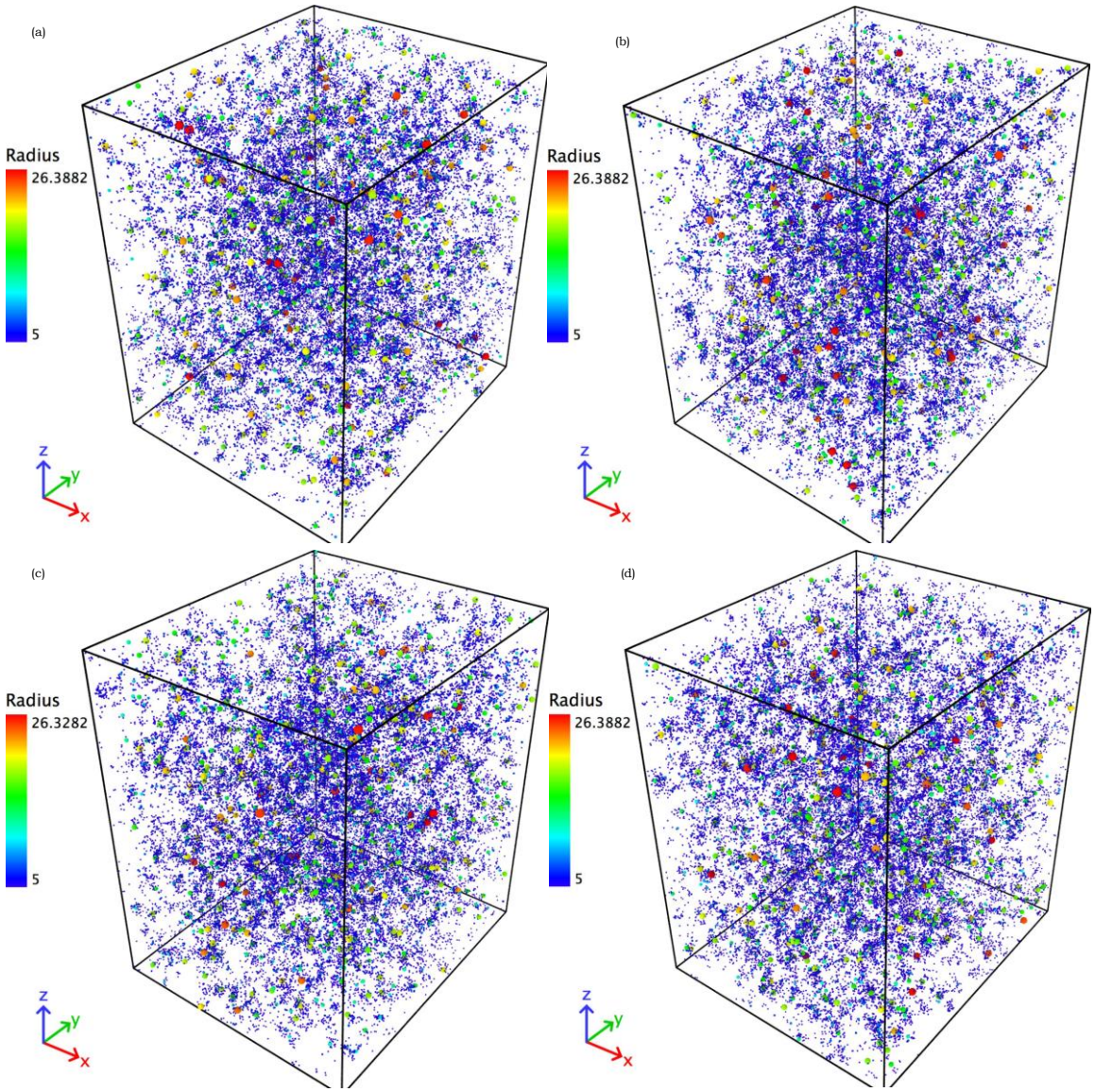

Figure 2. Snap shots of vacancy clusters in the simulation box (a) 10^{-5} dpa/s, 0.138 dpa (b) 10^{-6} dpa/s, 0.173 dpa (c) 10^{-7} dpa/s, 0.15 dpa (d) 10^{-8} dpa/s 0.130 dpa. (Vacancy Cluster Size = $(\text{Radius}/5)^3$).

Figure 3 (a), (b) and (c) shows plots of total number of vacancies, total number of vacancy clusters and average vacancy clusters size as a function of dose for 60, 75 and 100 keV cascades at 300 K for a dose rate of 10^{-6} dpa s^{-1}. As expected, the number density of vacancies increases with PKA energy due to increased defect production with PKA energy, Figure 3a. Larger clusters form at higher PKA energies resulting in a similar dose dependency of the number of vacancy clusters, Figure 3b. Figure 3(d) shows the fraction of surviving vacancies, which is a ratio of total number of vacancies present in the simulation cell and the total number of vacancies created, as a function of dose. It should be noted that the surviving fraction of vacancies for three PKA energies collapses into a single curve. This suggests that the rate of defect accumulation is independent of PKA energy of the cascade and depends primarily on the dose, at least for the PKA energies and doses shown in this report.

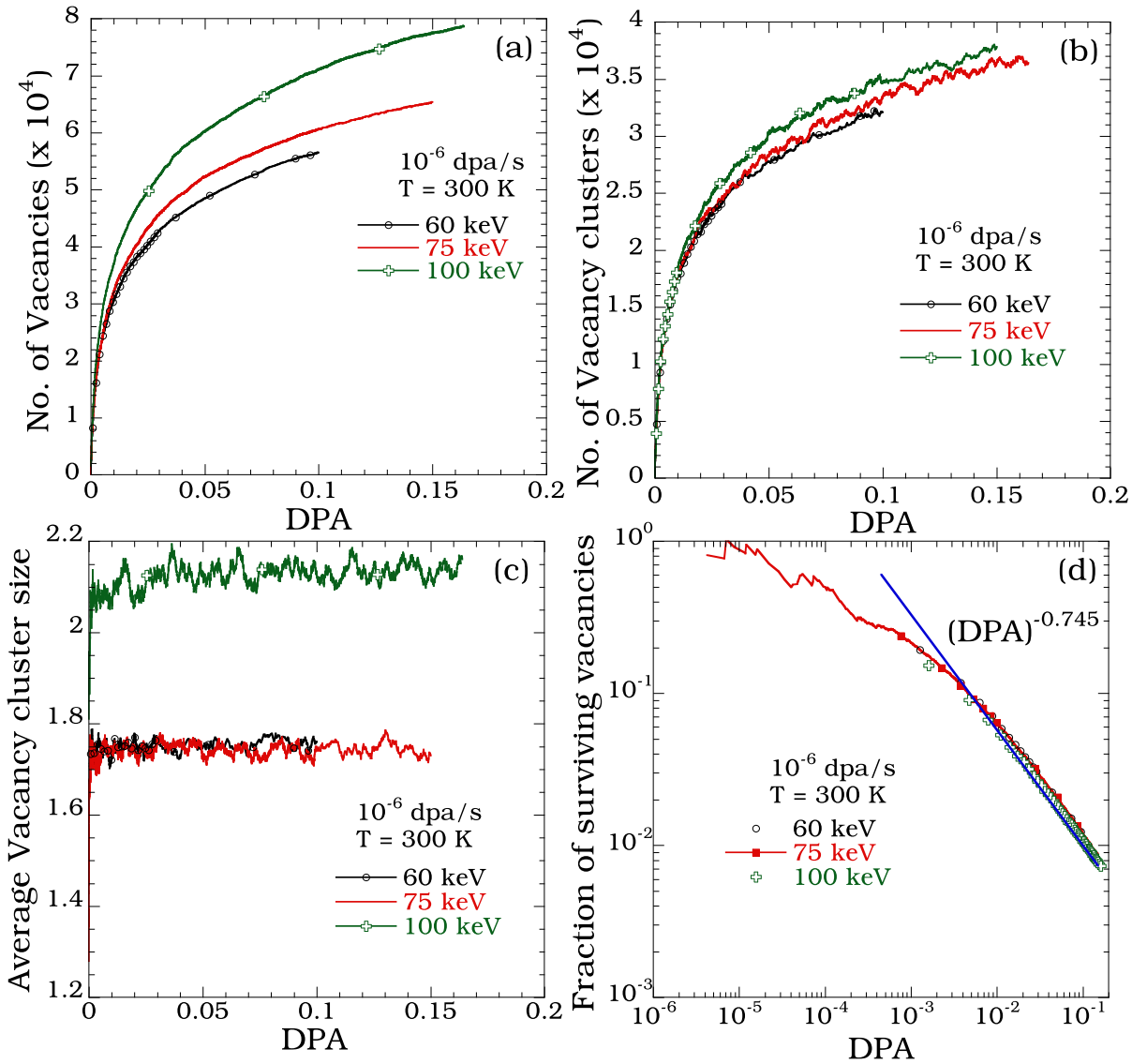

Figure 3. Comparison of damage accumulation at 10^{-6} dpa s^{-1} for 60, 75 and 100 keV cascades at 300 K as a function of dose (a) Number density of vacancies (b) Number density of vacancy clusters (c) average vacancy cluster size (d) fraction of surviving vacancies.

Future Work

Further simulations will be carried out to understand defect accumulation at various dose rates, PKA energies, temperatures, simulation cell and grain size, and also for different PKA spectra. In addition we sensitivity studies will be carried out to understand the effects of kinetic parameters and, in-cascade SIA and vacancy clustering.

Acknowledgement

All computations were performed on CARVER at National Energy Research Scientific Computing Center (NERSC) and Argonne National Lab, MCS Workstations

References

[1] G. Nandipati *et al* Semiannual Progress Report DOE/ER-0313/54, June 2013, 179-183
[2] W. Setyawan *et al* Semiannual Progress Report DOE/ER-0313/54, June 2013, 200-204
[3] C. S. Becquart *et al.* J. Nucl. Mater. 403 (2010) 75
[4] T.Faney, N.Juslin, B.D.Wirth,(*private communication)*.
[5] N.Juslin, B.D.Wirth, J. Nucl. Mater. 432(2013)61.
[6] D. A. Trentyev, L. Malerba, M. Hou, Phys. Rev. B 75 (2007) 104108.
[7] M.J. Norgett, M.T. Robinson, I.M. Torrens, Nucl. Eng. Des. 33 (1975) 50.